atmosphere

MDPI

Article

Intercomparison of Multiple Satellite Aerosol Products against AERONET over the North China Plain

Xuehua Fan *, Xiangao Xia and Hongbin Chen

Key Laboratory of Middle Atmosphere and Global Environment Observation, Institute of Atmospheric Physics, Chinese Academy of Sciences, Beijing 100029, China

* Correspondence: fxh@mail.iap.ac.cn

Received: 12 July 2019; Accepted: 20 August 2019; Published: 21 August 2019

Abstract: In this study, using Aerosol Robotic Network aerosol optical depth (AOD) products at three stations in the North China Plain (NCP)—a heavily polluted region in China—the AOD products from six satellite-borne radiometers: the Moderate Resolution Imagining Spectroradiometer (MODIS), the Multiangle Imaging Spectroradiometer (MISR), Ozone Mapping Imaging (OMI), the Visible Infrared Imaging Radiometer (VIIRS), the Sea-Viewing Wide Field-of-View Sensor (SeaWiFS), and Polarization and Directionality of the Earth's Reflectances (POLDER), were thoroughly validated, shedding new light on their advantages and disadvantages. The MODIS Deep Blue (DB) products provide more accurate retrievals than the MODIS Dark Target (DT) and other satellite products at the Beijing site (BJ, a megacity), with higher correlations with AERONET ($R > 0.93$), lower mean absolute bias ($MB < 0.012$), and higher percentages (>68%) falling within the expected error (EE). All MODIS DT and DB products perform better than the other satellite products at the Xianghe site (XH, a suburb). The MODIS/Aqua DT products at both 3-km and 10-km resolutions performed better than the other space-borne AOD products at the Xinglong site (XL, a rural area at the top of a mountain). MISR, VIIRS, and SeaWiFS tend to underestimate high AOD values and overestimate AOD values under very low AOD conditions in the NCP. Both OMI and POLDER significantly underestimate the AOD. In terms of data volume, MISR with the limited swath width of 380 km has less data volume than the other satellite sensors. MODIS products have the highest sampling rate, especially the MODIS DT and DB merged products, and can be used for various climate study and air-quality monitoring.

Keywords: aerosol optical depth of satellite; evaluation; North China Plain

1. Introduction

Atmospheric aerosols play a critical role in the earth–climate system. Aerosols influence Earth's energy budget by scattering and absorbing solar and terrestrial radiation or by modifying the cloud properties and precipitation patterns [1]. They also affect the atmospheric chemistry process and air quality. Aerosol forcing has been identified as one of the greatest uncertainties in our understanding of the global climate system due to the high variability in concentration, size, composition, shape, and optical properties [2,3].

Global and local aerosol properties have been extensively observed using various satellite radiometers during the last decades. Early satellite-borne sensors, such as the Advanced Very High Resolution Radiometer (AVHRR), have provided a nearly 25-year continuous record of global AOD values over the ocean [4]. Satellite AOD retrieval has benefited from advances in the satellite spectral, spatial, and angular resolutions of satellite-borne radiometers, which have made AOD retrieval over land possible and resulted in multiple AOD products, such as those from the Sea-viewing Wide

Field of View Sensor (SeaWiFS), the Moderate Resolution Imagining Spectroradiometer (MODIS), the Multiangle Imaging Spectroradiometer (MISR), Polarization and Directionality of the Earth's Reflectances (POLDER), Ozone Mapping Imaging (OMI), and the Visible Infrared Imaging Radiometer (VIIRS). Although much progress has been made in satellite remote sensing of aerosols during recent years, it is still challenging to retrieve precise AOD values with these passive satellites over land because of the complex coupling of the atmosphere and Earth's surface. Therefore, the comprehensive and systematic validation of satellite aerosol retrievals using high-quality ground measurements is essential for scientific and operational applications of satellite aerosol products [5]. All the aerosol properties and distributions should be quantified accurately to better understand the complex effects of aerosols in the atmosphere. Numerous studies have individually assessed aerosol products from the AVHRR [6,7], TOMS [8], MODIS [9–11], SeaWiFS [12], OMI [13], POLDER [14,15], MISR [16], and the latest VIIRS [5,17]. The instrument design and calibration, cloud masks, retrieval algorithms, underlying assumptions, and uncertainties involved in determining aerosol properties with the different satellite sensors vary [18], resulting in significant inconsistencies and gaps in aerosol products for different sensors. Even different AODs are derived from the same sensor using different retrieval algorithms, for example, AODs from the Dark Target (DT) and Deep Blue (DB) algorithms for the MODIS differ in not only their values but also their sampling rate [19]. Therefore, the differences between diverse satellite AOD products must be quantified, and this will be beneficial for the evaluation of regional aerosol radiative forcing and air quality and pollution transport studies, especially in regions with high aerosol loadings and complicated aerosol compositions.

Unprecedented economic development and population growth in the North China Plain (NCP) have taken place over the past four decades, resulting in considerably increased aerosol loading. The aerosol composition and sources there are very complex and include not only fine aerosol particles from human activities, but also coarse dust particles transported from remote dust source regions, which has been revealed by careful analysis of Aerosol Robotic Network (AERONET) aerosol products [20,21]. Three long-term AERONET sites have been established at distinct locations—Beijing (a megacity), Xianghe (a suburb), and Xinglong (a rural area at the top of a mountain)—which makes it possible to investigate and evaluate the aerosol properties from diverse satellite sensors.

The aim of this paper is to synthetically compare and evaluate multiple satellite AOD products over the NCP using AERONET data, which is expected to provide constructive suggestions on suitable satellite AOD products for specified tasks. Satellite aerosol products derived from SeaWiFS, MODIS, MISR, POLDER, OMI, and VIIRS are validated under the same conditions. The paper is structured as follows. In the next section, we introduce the study sites and the data. Section 3 is devoted to the aerosol optical property results at the three AERONET sites and their comparison against satellite products. The concluding remarks are given in Section 4.

2. The Study Sites and Data

2.1. Description of the Study Sites

Figure 1 shows the locations of the three AERONET stations. Beijing (BJ: 39.98°N, 116.38°E, 92.0 m above sea level (ASL)), which is situated at the northern tip of the NCP, is the Capital of China and had a population of over 21 million as of 2018. Beijing is surrounded by the Xishan and Yanshan Mountain ranges from the west to the northeast and includes heavily industrialized areas from the southwest to the east.

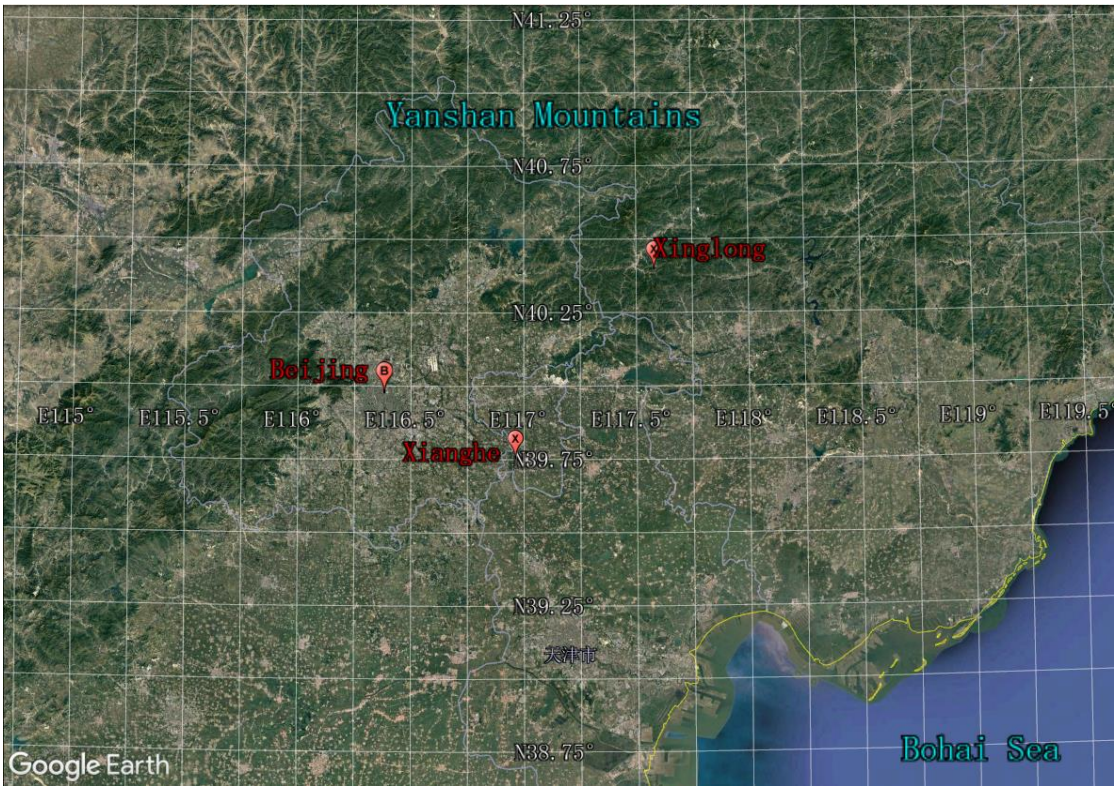

Figure 1. Google Earth map of the three AERONET (AErosol RObotic NETwork) sites: urban Beijing (BJ: 39.98°N, 116.38°E, 92.0 m above sea level), suburban Xianghe (XH: 39.75°N, 116.96°E, 36.0 m ASL), and rural Xinglong (XL: 40.40°N, 117.58°E, 920.0 m ASL).

Xianghe (XH: 39.75°N, 116.96°E, 36.0 m ASL), with a population of 350,000, is a county in the Hebei Province and is situated between the two megacities of Beijing and Tianjin. The observation site is surrounded by cropland, densely occupied residences, and light industry. The demand for heating and associated combustion activities increases in winter when coal-fueled boilers and coal-burning stoves are used for households [22].

Xinglong (XL: 40.40°N, 117.58°E, 970.0 m ASL) is an atmospheric background observation station of the Chinese Academy of Sciences and is situated at the top of a mountain. Situated 150 km from Beijing to the northeast, XL is located at the edge of a rapidly developing metropolitan area and is thus taken to be an atmospheric background station.

2.2. AERONET Data

The AERONET is a ground-based sun and sky scanning radiometer network that measures aerosol optical properties across the world. Aerosol optical and microphysical properties in the AERONET database include the aerosol optical depth (AOD), Angstrom exponent (AE), refractive index, size distribution, single scattering albedo (SSA), absorption AOD, and asymmetry factor. Aerosol properties are derived from the direct and diffuse solar spectral radiance measured by CIMEL CE318 sun-photometers. BJ, XH, and XL became permanent AERONET sites in April 2002, September 2004, and February 2006, respectively. The level 2 products of AERONET version 3 used in the study are automatically cloud cleared and quality assured, with prefield and postfield calibration applied. The AERONET AOD at 550 nm was computed using the quadratic fit on a log–log scale for comparing with data from the multiple satellite sensors. The accuracy of AERONET AODs is 0.01–0.02 in the visible and near-infrared wavelengths. The uncertainty of the SSA, which increases as the optical thickness decreases, is 0.03–0.07, depending on the AOD and the aerosol types [23].

2.3. MAPSS Data

The Multisensor Aerosol Products Sampling System (MAPSS) is a framework that provides statistics of spatial and temporal subsets of Level-2 aerosol scientific data sets (SDS) from a range of sensors that currently includes AERONET, MODIS, MISR, OMI, SeaWiFS, POLDER, and VIIRS. The data system was described in detail by Petrenko et al. [18]. The AERONET measurement sites were identified as focal points for spatial statistics. The process of generating the statistics for each spatial spaceborne aerosol product involves extracting the values of the pixels that fall within a circle with a diameter of approximately 55 km centered on the chosen AERONET site. Similarly, statistics for ground-based temporal observations in a particular station are derived from measurements taken within ±30 min of each satellite overpass over this location. All the satellite AOD pixels are filtered by quality assurance (QA) [24].

The MAPSS MODIS aerosol products include six datasets for version 060, i.e., DT and DB AODs at 10 km and DT AODs at 3 km from the twin MODIS onboard Terra and Aqua. MISR AODs (550 nm, version 0022) at a spatial resolution 17.6 km were used to collocate ground-based AERONET observations in MAPSS. The SeaWiFS onboard SeaStar satellite platform was originally designed for ocean color retrieval. It features a higher calibration precision and long-term stability in the radiometric measurements compared to the other sensors [25]. The latest SeaWiFS version 004 dataset at a spatial resolution of 13.5 km is employed in the MAPSS. OMI, which is onboard the Aura satellite, is capable of retrieving aerosol absorption, extinction optical depth and single scattering albedo data [26]. OMI 500-nm AODs of version 003 at 13.7×23.7 km^2 were used. Aerosol products from the POLDER, which is onboard a CNES/Myriade microsatellite PARASOL within the A-train constellation (December 2004–October 2013), were included. Level 2 POLDER aerosol data consist of AODs at 865 nm over land from multispectral and multiviewing-angle polarization measurements. These parameters have been averaged on a 3×3 level 1 pixel size area, leading to a spatial resolution of approximately 20×20 km^2 on the ground. The 550-nm AODs of version 001 at a spatial resolution of 6 km from the VIIRS/S-NPP (Suomi National Polar-orbiting Partnership) were used in the study.

3. Results

3.1. Seasonality of AERONET Aerosol Optical Properties

The intra-annual variabilities of the AERONET AOD, SSA, and FMF (Fine Mode Fraction) values at BJ, XH, and XL are represented as box-and-whiskers plots in Figure 2. The AOD, SSA, and FMF values at the three sites show distinct seasonality. The AOD values show a significant seasonality, with the maximum in the spring and summer and the minimum in the winter (DJF). The seasonality over the NCP has been revealed by numerous studies [20,21,27]. It can be seen that the atmosphere is typically the most turbid and the most variable with the widest distribution in summer (Figure 2a). The surface relative humidity and temperature are high in summer, which promotes the conversion of gas to particulate and results in higher AOD. The AOD showed higher values in June, July, and October at the three sites, which is related to regional open stalk burning during the harvest season [22,27]. This can also be seen by the MODIS fire products [28,29]. Higher AOD values in the spring are mainly caused by increasing coarse-mode dust particles transported from remote dust regions [21,27,30], which agrees with the lower FMF in the spring, as shown in Figure 2c.

It is obvious that the AOD values at BJ are much higher than those at the two other sites. The AOD values at the XL station were the lowest among the three sites. In contrast, the SSA values at XL were generally the highest among the three sites except in July and August, when data samples were insufficient due to the high frequency of cloud contamination and instrument breakdown. The two inversion products, SSA and FMF, showed a larger dispersion at XL than at BJ and XH because the retrieval uncertainty of SSA and FMF increases as the AOD values decrease. It can be seen in Figure 2a that the majority of the AOD values at XL are less than 0.4, the threshold of AERONET SSA inversion.

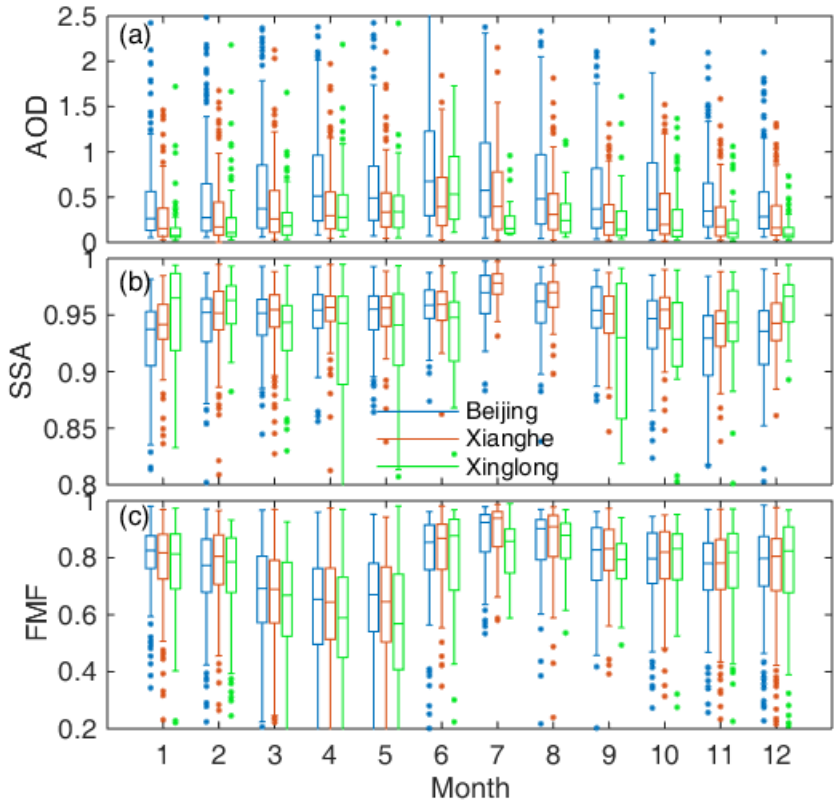

Figure 2. Statistical analysis showing monthly variation of AERONET AOD, Single Scattering Albedo (SSA), and fine mode fraction (FMF) values at Beijing (blue), Xianghe (firebrick), and Xinglong (lime) sites. The ends of each box denote the 25th and 75th percentiles of the distribution, the ends of the whiskers represent the 5th and 95th percentiles, and the line across the box is the median of the distribution.

3.2. Results of Intercomparison

Table 1 shows the validation periods and evaluation metrics at the three sites, including the number of satellite and AERONET matchups, the mean bias (defined such that positive values indicate an overestimation of satellite retrieval), the linear correlation coefficient (R), the slope, and the intercept of linear regressions for the AODs retrieved by satellite versus the AERONET AODs, and the percentages of the satellite AODs falling within the reference expected error (EE), above the EE, and below the EE. For consistency among the different aerosol products, we used the EE of the MODIS C5 aerosol product over land ±(0.05 + 0.15AOD) in the study. Furthermore, the Taylor diagrams, as shown in Figure 3, were employed to visualize the degree of correspondence between the various satellite AOD products and the AERONET AOD measurements in terms of their correlation, their centered root-mean-square difference, and the ratio of their variances. R is represented by the polar angle, the centered root-mean-square difference (CRMSD) is denoted by the radial lines labeled by the cosine of the angle made with the abscissa, and the standard deviation is normalized by the standard deviation of AERONET (NSD), as shown by the radius, and all are indicated by a single point on a two-dimensional (2-D) plot in the Taylor diagram. A detailed description of the Taylor diagram is given by Taylor [31].

Table 1. The validation periods and data statistics at the Beijing, Xianghe, and Xinglong sites, including the number of satellites and AERONET (Aerosol Robotic NETwork) matchups, the mean bias (defined such that positive values indicate an overestimation of satellite retrieval), the root mean square difference (RMSD), the linear correlation coefficient (R), the slope and the intercept of linear regression, and the percentages of satellite AODs falling within the expected error (EE), above the EE, and below the EE.

Sites	Validation Period	Dataset	Collocated Number	Mean Bias	RMSD	Percentage Falling within the EE	Percentage Falling above the EE	Percentage Falling below the EE	R	Slope	Intercept
Beijing	May 2002 to May 2017	MISR	242	−0.081	0.195	78.51%	2.07%	19.42%	0.939	0.535	0.085
		TMOD3km DT	1163	0.151	0.183	39.38%	58.30%	2.32%	0.933	0.960	0.169
		AMOD3km DT	846	0.14	0.197	39.48%	55.32%	3.90%	0.903	0.917	0.168
		TMOD10km DT	1121	0.164	0.198	34.88%	58.59%	6.53%	0.918	0.895	0.211
		TMOD10km DB	1907	0.012	0.204	68.17%	22.71%	12.95%	0.932	0.921	0.050
		AMOD10km DT	934	0.143	0.173	36.95%	59.71%	3.34%	0.923	0.909	0.183
		AMOD10km DB	1768	−0.002	0.195	72.17%	14.14%	13.69%	0.934	0.921	0.036
		OMI	600	−0.052	0.202	57.00%	19.50%	23.50%	0.832	0.576	0.114
		SeaWiFS	405	0.010	0.109	70.12%	22.47%	7.41%	0.896	0.719	0.090
	May 2002 to Oct. 2013	POLDER	548	−0.213	0.251	24.64%	0.00%	75.36%	0.776	0.262	0.017
	May 2002 to May 2018	VIIRS	536	0. 042	0.254	49.81%	37.31%	12.87%	0.848	0.742	0.157
Xianghe	Sep. 2004 to May 2017	MISR	169	−0.095	0.240	70.41%	4.14%	25.44%	0.923	0.553	0.087
		TMOD3kmDT	837	0.070	0.187	67.98%	29.63%	2.39%	0.953	1.047	0.047
		AMOD3kmDT	684	0.039	0.146	73.10%	20.18%	6.73%	0.971	1.096	−0.005
		TMOD10km DT	677	0.062	0.170	71.34%	26.29%	2.36%	0.958	1.010	0.057
		TMOD10km DB	1171	0.066	0.245	63.36%	30.83%	5.81%	0.922	0.953	0.091
		AMOD10km DT	445	0.037	0.131	73.93%	19.10%	6.97%	0.972	1.070	0.004
		AMOD10km DB	1101	0.067	0.241	64.40%	28.43%	7.18%	0.921	1.014	0.060
		OMI	473	−0.095	0.171	58.14%	5.71%	36.15%	0.876	0.599	0.047
		SeaWiFS	340	0.039	0.208	65.29%	28.82%	5.88%	0.847	0.670	0.144
	Sep. 2004 to May 2012	POLDER	494	−0.208	0.243	25.51%	0.00%	74.49%	0.841	0.295	0.012
	Sep. 2004 to May 2018	VIIRS	722	−0.057	0.246	58.86%	15.10%	26.04%	0.890	0.752	0.073
Xinglong	Feb. 2006 to Dec. 2015	MISR	23	−0.028	0.083	86.96%	4.35%	8.70%	0.921	0.632	0.047
		TMOD3kmDT	470	0.002	0.141	79.15%	14.26%	6.66%	0.757	0.730	0.056
		AMOD3kmDT	313	−0.023	0.101	73.80%	7.67%	18.53%	0.885	1.021	-0.027
		TMOD10km DT	342	0.001	0.162	78.65%	14.46%	7.31%	0.742	0.765	0.050
		TMOD10km DB	750	0.056	0.209	67.2%	28.13%	4.67%	0.756	1.102	0.037
		AMOD10km DT	156	−0.019	0.117	71.15%	7.69%	21.15%	0.868	0.984	-0.015
		AMOD10km DB	558	−0.026	0.165	72.58%	18.82%	8.60%	0.855	1.250	-0.024
		OMI	311	−0.008	0.132	62.38%	17.04%	20.58%	0.816	0.791	0.037
		SeaWiFS	105	−0.016	0.082	82.86%	5.71%	11.43%	0.820	0.555	0.051
	Feb. 2006 to May 2012	POLDER	225	−0.126	0.123	37.33%	0.00%	62.67%	0.601	0.234	0.007
	Feb. 2006 to May 2018	VIIRS	122	−0.001	0.116	64.75%	21.31%	13.93%	0.867	0.771	0.053

MISR: the Multiangle Imaging Spectroradiometer; TMOD3kmDT: the Moderate Resolution Imagining Spectroradiometer (MODIS)/Terra AOD from Dark Target algorithm at 3 km; AMOD3kmDT: the MODIS/Aqua AOD from Dark Target algorithm at 3 km; TMOD10kmDT: the MODIS/Terra AOD from Dark Target algorithm at 10 km; TMOD10kmDB: the MODIS/Terra AOD from Deep Blue algorithm at 10 km; AMOD10kmDT: the MODIS/Aqua AOD from Dark Target algorithm at 10 km; AMOD10kmDB: the MODIS/Aqua AOD from Deep Blue algorithm at 10 km; OMI: Ozone Mapping Imaging; SeaWiFS: the Sea-Viewing Wide Field-of-View Sensor; POLDER: the Polarization and Directionality of the Earth's Reflectances; VIIRS: the Visible Infrared Imaging Radiometer.

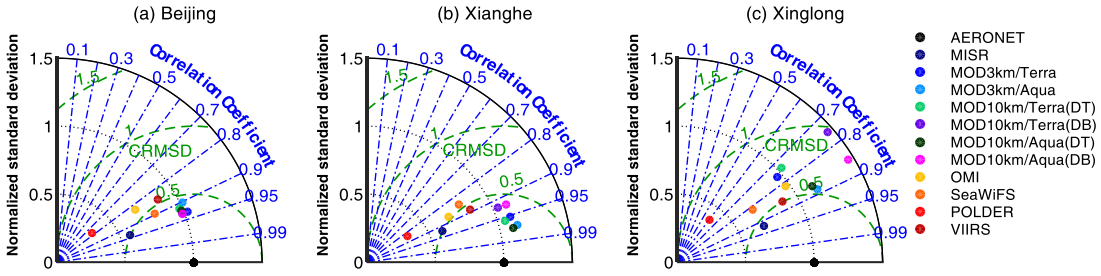

Figure 3. Pattern statistics of Taylor diagrams comparing satellite retrievals and AERONET observations in terms of monthly mean AODs at the (**a**) Beijing, (**b**) Xianghe, and (**c**) Xinglong sites.

At the BJ site, both the MODIS/Terra and MODIS/Aqua DB AOD products showed better agreement with the AERONET AODs compared to the other satellite AODs. The two AOD products had higher correlations with AERONET ($R > 0.93$) and a lower mean absolute bias ($MB < 0.01$). The NSDs of MODIS DB AOD retrievals were approximately 0.99, suggesting that the MODIS DB AODs are capable of capturing the temporal variation of the AERONET AODs. In addition, the percentages of all data points falling within the EE were close to or greater than one standard deviation (~68%) for the MODIS/Terra, MODIS/Aqua DB AODs. The linear regression slopes were approximately 0.92, and the intercepts were close to zero. Despite the high correlations ($R > 0.90$) between the AERONET AODs and all the MODIS DT AOD products, the fractions of all matchups within the EE were less than 40%, and the MB values were up to ~0.15.

The MODIS/Aqua DT products at resolutions of 3-km and 10-km performed better than other space-borne AOD products at the XH and XL sites, although the statistical point at the XL site depart farther from AERONET reference position than those at the BJ and XH sites. This was evidenced by higher correlations ($R > 0.97$ and $R > 0.86$ at the XH and XL sites, respectively) and lower root-mean-square differences ($RMSD < 0.15$ and $RMSD < 0.12$ at the XH and XL sites, respectively). Values of the linear regression slope were very close to 1, and the absolute values of the intercepts were less than 0.03. The percentages of the MODIS/Aqua DT AODs falling within the EE exceeded 71%. The MODIS/Terra DT, MODIS/Terra, and MODIS/Aqua DB AODs also showed good agreement with the AERONET AODs at the XH site. The values of the correlation coefficients exceeded 0.92. The linear fitting slopes were close to 1, and the intercepts were less than 0.1. The MODIS/Terra DT products generally underestimated the AODs at the XL site although a high percentage of matchup data fell with the EE (79.15% and 78.65% for the MODIS/Terra AODs at resolutions of 3-km and 10-km, respectively). The MODIS/Terra and MODIS/Aqua DB products showed a significant overestimation of the AODs at the XL site. The statistical points of the MODIS DB AOD retrievals at the XL site were the farthest from the AERONET reference point for the three sites (Figure 3), which shows that the MODIS DB products experience a remarkable degradation at the XL site.

The MISR retrievals significantly underestimated the AODs at the BJ and XH sites, although the MISR AODs had high correlations ($R > 0.92$) with the AERONET AODs and high percentages of falling within the EE (78.51% and 70.41% at the BJ and XH sites, respectively). The MISR AOD products showed negative MB values (-0.08 and -0.10 at the BJ and XH sites, respectively), with lower standard deviations (0.57 and 0.60 at the BJ and XH sites, respectively) compared to the AERONET AODs. There are only 23 collocated MISR and AERONET samples at the XL site, which is insufficient for significant statistical analysis.

The scatter plots of the OMI AODs, SeaWiFS AODs, and VIIRS AODs against the AERONET AODs are given in Figure 4. The correlation coefficients between the OMI and AERONET AODs were 0.83, 0.88, and 0.82 at the BJ, XH, and XL sites, respectively, and the MB values were negative at the three sites. The slopes of the linear regression between the OMI and AERONET AODs were less than 0.60 at the BJ and XH sites, and the intercepts were 0.11 and 0.05 at the BJ and XH sites, respectively. The NSD values of the OMI AODs were lower than those of the AERONET AODs at the BJ and XH sites (Figure 3a,b). The OMI performed better at the XL site than at the BJ and XH sites,

with a higher slope (0.791), a lower intercept (0.037), and a standard deviation very close to that of AERONET (Figure 3c). However, all the statistics suggest that the OMI significantly underestimates the AOD when aerosol loading is medium or high and slightly overestimates the AOD when the AOD is very low. The worse performance of the OMI in the urban area is caused by the combined effect of complex surface characterization, cloud contamination, and possibly aerosol model representation. Aerosol loading and clouds are highly variable within the large OMI footprint for the urban area, which results in a diminishment of the retrieval quality.

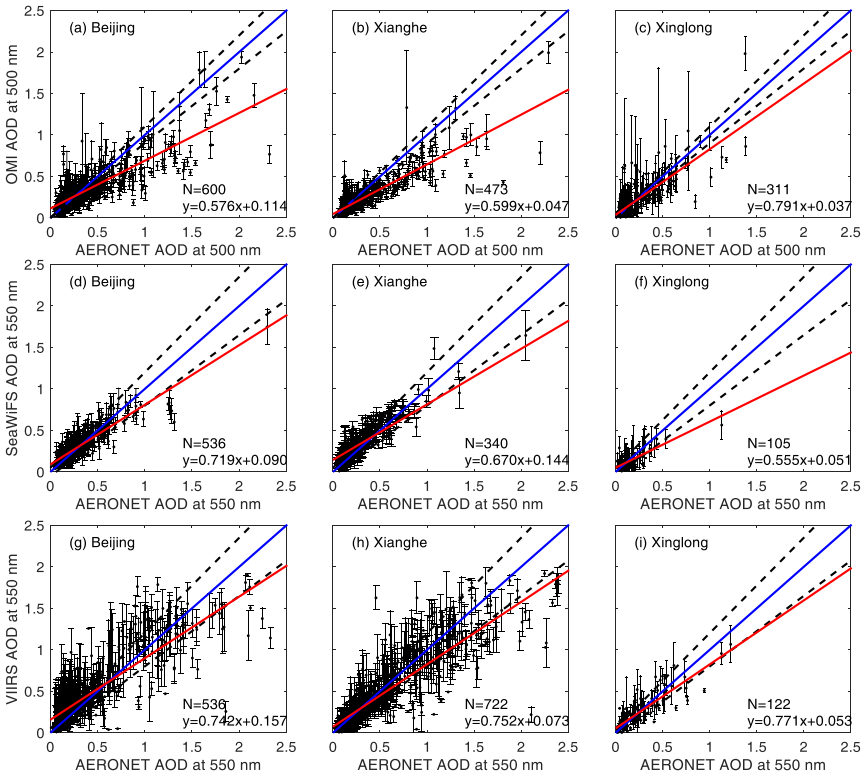

Figure 4. Scatter plots representing the evaluation of OMI (the Ozone Mapping Imaging) (**a**–**c**), SeaWiFS (the Sea-Viewing Wide Field-of-View Sensor) (**d**–**f**), and VIIRS (the Visible Infrared Imaging Radiometer) (**g**–**i**) AODs against the ground-based AERONET AODs at the Beijing, Xianghe, and Xinglong sites. The solid red and blue lines represent the linear regression and 1:1 fitting lines, respectively. The dashed black lines indicate the uncertainty envelopes with 0.1 AOD for OMI and ±0.05 + 0.15 AOD for SeaWiFS and VIIRS.

The percentages of the SeaWiFS AOD data falling within the EE were 70.12%, 65.29%, and 82.86%, the correlation coefficients are 0.90, 0.84, and 0.82, and the RMSD values were 0.109, 0.208, and 0.082 at the BJ, XH, and XL sites, respectively. The standard deviations of the SeaWiFS AOD were less than those of AERONET (the NSDs were 0.81, 0.79, and 0.68 for the BJ, XH, and XL sites, respectively). The slopes (intercepts) of the linear regression were 0.72 (0.09), 0.67 (0.14), and 0.56 (0.05) at the BJ, XH, and XL sites, respectively, which shows that the SeaWiFS retrievals underestimate certain high-AOD events.

The VIIRS AOD products performed slightly better at the XL site than at the BJ and XH sites. The RMSD was reduced from approximately 0.25 at the BJ and XH sites to 0.12 at the XL site. The percentage of VIIRS AOD retrievals falling within the EE at the XL site (64.75%) was the highest among the three sites, although it was lower than the previous global evaluation of VIIRS EDR AODs over land with a value of 71% [5]. The slopes (intercepts) of the linear regression were 0.74 (0.16), 0.75 (0.07), and 0.771 (0.053) at the BJ, XH, and XL sites, respectively, which also indicates that VIIRS underestimates certain high-AOD events and overestimates AODs under relatively low-AOD conditions.

Although the correlations between the space-borne AOD retrievals and the AERONET AODs degraded (R < 0.90) at the XL site, the RMSD and MB values were reduced at the XL site compared to those at the BJ and XH sites. In addition, the percentages of matchup data falling within the EE were higher at the XL site than those at the BJ and XH sites for all the satellite AOD products. This result is due to the variation range of AOD at XL being much smaller than that at the BJ and XH sites (Figure 2a).

The aerosols in the NCP are a mixture of coarse-mode and fine-mode particles [27]. The coarse-mode dust aerosols increase significantly in the NCP in the spring, which can be seen from the lower FMF values shown in Figure 2c. However, the POLDER polarization measurements are sensitive to fine-mode particles over land [15,32], which results in POLDER underestimations of the AOD (negative MB values and lower percentages of POLDER AODs within the EE (<40%)).

4. Concluding Remarks

Based on ground-based AERONET observations, various satellite AOD products were evaluated for the NCP. The MODIS DB products provide more accurate retrievals than the MODIS DT and other space-borne AOD products at the BJ site, which suggests that the DB algorithm is suitable for the urban surface. All MODIS DT and DB products perform better than the other satellite products at the XH site. The MODIS/Aqua DT products at resolutions of 3-km and 10-km perform better than the other space-borne AOD products at the XL site. The MODIS 3-km DT algorithm uses the same protocol as the 10-km DT [33], so the two MODIS AOD products perform consistently at the three sites except that the 3-km products have a higher sampling rate. However, the MODIS DB products perform worse at the XL site than at the BJ and XH sites. Several factors lead to this degradation. The XL site is situated on a mountain top with an elevation of 960 m, and the surrounding topography and surface types are complex and inhomogeneous, which results in an inadequacy in the spatial representation of AERONET observations. Moreover, there are remarkable differences in the absorption and size properties between the BJ and XL sites, as shown in Figure 2b,c. Polluted and clean urban aerosols are dominant at the BJ site, and in addition, smoke and dust aerosols account for approximately 45% of the total (dust aerosol loading increases in the spring). The proportion of urban aerosols is reduced, and high absorption smoke aerosols increase at the XL site [17]. The aerosol model types used in the retrieval algorithm of MODIS AODs remain unchanged over the NCP. The uncertainty in the aerosol model type also results in a degraded retrieval accuracy of the MODIS AOD.

The MISR, VIIRS, and SeaWiFS tend to underestimate certain high-AOD events and overestimate AODs under very low-AOD conditions for the NCP. The OMI significantly underestimates the AOD for the NCP and slightly overestimates the AOD when the AOD is low (<0.20) at the BJ site. The POLDER polarization measurements are sensitive to fine-mode particles over land [15,32], which results in POLDER underestimation of the AODs for the NCP.

The relative data volume differences among the various data products should be carefully considered when interpreting and evaluating the statistics of the AOD products in this study. The sensor swath width is one of main factors that determine the available volume of data. The MISR, with a limited swath width of 380-km, has less data volume than the other satellite sensors. In addition, the seasonal changes in the retrieval conditions also have a considerable impact on the data volume [24]. The XL site has less matchup data points than the BJ and XH sites due to the limited time period of AERONET measurements at the XL site. MODIS 3 km products with the highest spatial resolution and relative high sampling rate can be used for various climate study and air-quality monitoring. However, the sampling rate of MODIS 3-km AOD products derived from DT algorithm decreases significantly on the NCP in winter. The MODIS DB AOD products complement the MODIS DT AOD coverage, especially in winter [19]. The MODIS DT and DB merged products show a larger sampling rate, which is more suitable for air-quality monitoring.

Author Contributions: X.X. and H.C. conceived of the presented idea, designed the manuscript framework, and contributed to the interpretation of the results. X.F. processed the MAPSS and AERONET data, analyzed the results, and wrote the manuscript. All authors provided critical feedback and helped shape the analysis and manuscript.

Funding: This research was supported by the National Key R&D Program of China (No. 2017YFA0603504), and the National Natural Science Foundation of China (No.41475027, and 41775033).

Acknowledgments: The team of MAPSS data are thanked for providing the data. The authors thank Z.J. Song for providing the MODIS DT and DB merged AOD data. The authors would like to acknowledge two anonymous referees for their useful comments on the manuscript.

Conflicts of Interest: The authors declare no conflict of interest.

References

1. Chin, M.; Diehl, T.; Tan, Q.; Prospero, J.M.; Kahn, R.A.; Remer, L.A.; Yu, H.; Sayer, A.M.; Bian, H.; Geogdzhayev, I.V.; et al. Multi-decadal aerosol variations from 1980 to 2009, A perspective from observations and a global model. *Atmos. Chem. Phys.* **2014**, *14*, 3657–3690. [CrossRef]
2. Boucher, O.; Randall, D.; Artaxo, P.; Bretherton, C.; Feingold, G.; Forster, P.; Kerminen, V.M.; Kondo, Y.; Liao, H.; Lohmann, U.; et al. Clouds and Aerosols. In *Climate Change 2013: The Physical Science Basis*; Contribution of Working Group I to the Fifth Assessment Report of the Intergovernmental Panel on Climate Change; Stocker, T.F., Qin, D., Plattner, G.K., Tignor, M., Allen, S.K., Boschung, J., Nauels, A., Xia, Y., Bex, V., Midgley, P.M., Eds.; Cambridge University Press: Cambridge, UK; New York, NY, USA, 2013.
3. Yu, H.B.; Zhang, Z.B. New directions: Emerging satellite observations of above-cloud aerosols and direct radiative forcing. *Atmos. Environ.* **2013**, *72*, 36–40. [CrossRef]
4. Li, J.; Carlson, B.E.; Lacis, A.A. Revisiting AVHRR tropospheric aerosol trends using principal component analysis. *J. Geophys. Res.-Atmos.* **2014**, *119*, 3309–3320. [CrossRef]
5. Huang, J.F.; Kondragunta, S.; Laszlo, I.; Liu, H.Q.; Remer, L.A.; Zhang, H.; Superczynski, S.; Ciren, P.; Holben, B.N.; Petrenko, M. Validation and expected error estimation of Suomi-NPP VIIRS aerosol optical thickness and Angstrom exponent with AERONET. *J. Geophys. Res.-Atmos.* **2016**, *121*, 7139–7160. [CrossRef]
6. Zhao, T.X.P.; Laszlo, I.; Guo, W.; Heidinger, A.; Cao, C.; Jelenak, A.; Tarpley, D.; Sullivan, J. Study of long-term trend in aerosol optical thickness observed from operational AVHRR satellite instrument. *J. Geophys. Res.-Atmos.* **2008**, *113*. [CrossRef]
7. Li, Z.; Zhao, X.; Kahn, R.; Mishchenko, M.; Remer, L.; Lee, K.H.; Wang, M.; Laszlo, I.; Nakajima, T.; Maring, H. Uncertainties in satellite remote sensing of aerosols and impact on monitoring its long-term trend: A review and perspective. *Ann. Geophys.* **2009**, *27*, 2755–2770. [CrossRef]
8. Torres, O.; Bhartia, P.K.; Herman, J.R.; Sinyuk, A.; Ginoux, P.; Holben, B. A long-term record of aerosol optical depth from TOMS observations and comparison to AERONET measurements. *J. Atmos. Sci.* **2002**, *59*, 398–413. [CrossRef]
9. Remer, L.A.; Kaufman, Y.J.; Tanre, D.; Mattoo, S.; Chu, D.A.; Martins, J.V.; Li, R.R.; Ichoku, C.; Levy, R.C.; Kleidman, R.G.; et al. The MODIS aerosol algorithm, products, and validation. *J. Atmos. Sci.* **2005**, *62*, 947–973. [CrossRef]
10. Levy, R.C.; Remer, L.A.; Kleidman, R.G.; Mattoo, S.; Ichoku, C.; Kahn, R.; Eck, T.F. Global evaluation of the Collection 5 MODIS dark-target aerosol products over land. *Atmos. Chem. Phys.* **2010**, *10*, 10399–10420. [CrossRef]
11. Sayer, A.M.; Munchak, L.A.; Hsu, N.C.; Levy, R.C.; Bettenhausen, C.; Jeong, M.J. MODIS Collection 6 aerosol products: Comparison between Aqua's e-Deep Blue, Dark Target, and "merged" data sets, and usage recommendations. *J. Geophys. Res.-Atmos.* **2014**, *119*, 13965–13989. [CrossRef]
12. Sayer, A.M.; Hsu, N.C.; Bettenhausen, C.; Jeong, M.J.; Holben, B.N.; Zhang, J. Global and regional evaluation of over-land spectral aerosol optical depth retrievals from SeaWiFS. *Atmos. Meas. Tech.* **2012**, *5*, 1761–1778. [CrossRef]
13. Ahn, C.; Torres, O.; Jethva, H. Assessment of OMI near-UV aerosol optical depth over land. *J. Geophys. Res.-Atmos.* **2014**, *119*, 2457–2473. [CrossRef]
14. Goloub, P.; Tanre, D.; Deuze, J.L.; Herman, M.; Marchand, A.; Breon, F.M. Validation of the first algorithm applied for deriving the aerosol properties over the ocean using the POLDER ADEOS measurements. *IEEE Trans. Geosci. Remote Sens.* **1999**, *37*, 1586–1596. [CrossRef]

15. Fan, X.H.; Goloub, P.; Deuze, J.L.; Chen, H.B.; Zhang, W.X.; Tanre, D.; Li, Z.Q. Evaluation of PARASOL aerosol retrieval over North East Asia. *Remote Sens. Environ.* **2008**, *112*, 697–707. [CrossRef]
16. Kahn, R.A.; Nelson, D.L.; Garay, M.J.; Levy, R.C.; Bull, M.A.; Diner, D.J.; Martonchik, J.V.; Paradise, S.R.; Hansen, E.G.; Remer, L.A. MISR Aerosol Product Attributes and Statistical Comparisons With MODIS. *IEEE Trans. Geosci. Remote Sens.* **2009**, *47*, 4095–4114. [CrossRef]
17. Zhu, J.; Xia, X.G.; Wang, J.; Che, H.Z.; Chen, H.B.; Zhang, J.Q.; Xu, X.G.; Levy, R.C.; Oo, M.; Holz, R.; et al. Evaluation of Aerosol Optical Depth and Aerosol Models from VIIRS Retrieval Algorithms over North China Plain. *Remote Sens.* **2017**, *9*, 432. [CrossRef]
18. Petrenko, M.; Ichoku, C.; Leptoukh, G. Multi-sensor Aerosol Products Sampling System (MAPSS). *Atmos. Meas. Tech.* **2012**, *5*, 913–926. [CrossRef]
19. Song, Z.J.; Fu, D.S.; Zhang, X.L.; Han, X.L.; Song, J.J.; Zhang, J.Q.; Wang, J.; Xia, X.G. MODIS AOD sampling rate and its effect on PM2.5 estimation in North China. *Atmos. Environ.* **2019**, *209*, 14–22. [CrossRef]
20. Xia, X.G.; Chen, H.B.; Goloub, P.; Zong, X.M.; Zhang, W.X.; Wang, P.C. Climatological aspects of aerosol optical properties in North China Plain based on ground and satellite remote-sensing data. *J. Quant. Spectrosc. Radiat. Transf.* **2013**, *127*, 12–23. [CrossRef]
21. Fan, X.H.; Xia, X.A.; Chen, H.B. Comparison of Column-Integrated Aerosol Optical and Physical Properties in an Urban and Suburban Site on the North China Plain. *Adv. Atmos. Sci.* **2015**, *32*, 477–486. [CrossRef]
22. Li, C.; Marufu, L.T.; Dickerson, R.R.; Li, Z.Q.; Wen, T.X.; Wang, Y.S.; Wang, P.C.; Chen, H.B.; Stehr, J.W. In situ measurements of trace gases and aerosol optical properties at a rural site in northern China during East Asian Study of Tropospheric Aerosols: An International Regional Experiment 2005. *J. Geophys. Res.-Atmos.* **2007**, *112*. [CrossRef]
23. Dubovik, O.; Holben, B.; Eck, T.F.; Smirnov, A.; Kaufman, Y.J.; King, M.D.; Tanre, D.; Slutsker, I. Variability of absorption and optical properties of key aerosol types observed in worldwide locations. *J. Atmos. Sci.* **2002**, *59*, 590–608. [CrossRef]
24. Petrenko, M.; Ichoku, C. Coherent uncertainty analysis of aerosol measurements from multiple satellite sensors. *Atmos. Chem. Phys.* **2013**, *13*, 6777–6805. [CrossRef]
25. Hsu, N.C.; Gautam, R.; Sayer, A.M.; Bettenhausen, C.; Li, C.; Jeong, M.J.; Tsay, S.C.; Holben, B.N. Global and regional trends of aerosol optical depth over land and ocean using SeaWiFS measurements from 1997 to 2010. *Atmos. Chem. Phys.* **2012**, *12*, 8037–8053. [CrossRef]
26. Torres, O.; Tanskanen, A.; Veihelmann, B.; Ahn, C.; Braak, R.; Bhartia, P.K.; Veefkind, P.; Levelt, P. Aerosols and surface UV products from Ozone Monitoring Instrument observations: An overview. *J. Geophys. Res.-Atmos.* **2007**, *112*. [CrossRef]
27. Xia, X.A.; Chen, H.B.; Wang, P.C.; Zhang, W.X.; Goloub, P.; Chatenet, B.; Eck, T.F.; Holben, B.N. Variation of column-integrated aerosol properties in a Chinese urban region. *J. Geophys. Res.* **2006**, *111*. [CrossRef]
28. Fan, X.H.; Chen, H.B.; Xia, X.G.; Li, Z.Q.; Cribb, M. Aerosol optical properties from the Atmospheric Radiation Measurement Mobile Facility at Shouxian, China. *J. Geophys. Res.-Atmos.* **2010**, *115*. [CrossRef]
29. Xia, X.G.; Zong, X.M.; Sun, L. Exceptionally active agricultural fire season in mid-eastern China in June 2012 and its impact on the atmospheric environment. *J. Geophys. Res.-Atmos.* **2013**, *118*, 9889–9900. [CrossRef]
30. Che, H.Z.; Zhang, X.Y.; Chen, H.B.; Damiri, B.; Goloub, P.; Li, Z.Q.; Zhang, X.C.; Wei, Y.; Zhou, H.G.; Dong, F.; et al. Instrument calibration and aerosol optical depth validation of the China Aerosol Remote Sensing Network. *J. Geophys. Res.-Atmos.* **2009**, *114*. [CrossRef]
31. Taylor, K.E. Summarizing multiple aspects of model performance in a single diagram. *J. Geophys. Res.-Atmos.* **2001**, *106*, 7183–7192. [CrossRef]
32. Su, X.; Goloub, P.; Chiapello, I.; Chen, H.; Ducos, F.; Li, Z. Aerosol variability over East Asia as seen by POLDER space-borne sensors. *J. Geophys. Res.-Atmos.* **2010**, *115*. [CrossRef]
33. Remer, L.A.; Mattoo, S.; Levy, R.C.; Munchak, L.A. MODIS 3 km aerosol product: Algorithm and global perspective. *Atmos. Meas. Tech.* **2013**, *6*, 1829–1844. [CrossRef]